Effects of temperature and density on the two-nucleon momentum correlation function from excited single nuclei

Ting-Ting Wang(王婷婷),[1] Yu-Gang Ma(马余刚)*,[1,2] De-Qing Fang(方德清),[1,2] and Huan-Lin Liu(刘焕玲)[3]

[1]*Key Laboratory of Nuclear Physics and Ion-Beam Application (MOE), Institute of Modern Physics, Fudan University, Shanghai 200433, China*

[2]*Shanghai Research Center for Theoretical Nuclear Physics, NSFC and Fudan University, Shanghai 200438, China*

[3]*Shanghai Institute of Applied Physics, Chinese Academy of Sciences, Shanghai 201800, China*

(Dated: December 28, 2021)

Two-nucleon momentum correlation functions are investigated for different single thermal sources at given initial temperature (T) and density (ρ). To this end, the evolutions of various single excited nuclei at $T = 1 - 20$ MeV and $\rho = 0.2$ - 1.2 ρ_0 are simulated using the thermal isospin-dependent quantum molecular dynamics ($ThIQMD$) model. Momentum correlation functions of identical proton-pairs ($C_{pp}(q)$) or neutron-pairs ($C_{nn}(q)$) at small relative momenta are calculated by *Lednický* and *Lyuboshitz* analytical method. The results illustrate that $C_{pp}(q)$ and $C_{nn}(q)$ keep sensitivities to the source size (A) at lower T or higher ρ, but almost not at higher T or lower ρ. And the sensitivities become stronger for smaller source. Moreover, the T, ρ and A dependencies of the Gaussian source radii are also extracted by fitting the two-proton momentum correlation functions, and the results are consistent with the above conclusions.

PACS numbers:

I. INTRODUCTION

Properties of nuclear matter is one of the most interesting topics in heavy-ion physics [1–5] and lots of works have been done around zero temperature, including the nuclear equation of state (EOS). However, the studies on properties of nuclear matter at finite temperatures are relatively limited. Many previous works mainly focus on the temperature dependence of hot nuclear matter and the nuclear liquid-gas phase transition ($LGPT$) [6–15], the ratio between shear viscosity to entropy density (η/s) [16–20], as well as the nuclear giant dipole resonance [21–23] etc. Among above works, the relationship between the phase transition temperature and the source size has been investigated [6]. In Ref. [6], the finite-size scaling effects on nuclear liquid-gas phase transition probes are investigated by studying de-excitation processes of the thermal sources by the isospin-dependent quantum molecular dynamics model (IQMD). It explores several probes including the total multiplicity derivative, second moment parameter, intermediate mass fragment multiplicity, $Fisher's$ power-law exponent as well as $Ma's$ nuclear $Zipf's$ law exponent, and obtains the phase transition temperatures from them. Recently, the deep neural network has also been used to determine the nuclear liquid gas phase transition [24] and estimate the temperature of de-excited nuclei by the charge multiplicity distribution [25]. The latter work proposes the charge multiplicity distribution can be used as a thermometer of heavy-ion collisions.

Considering that the intermediate-state at high temperature and density in the evolution process of nuclear reactions cannot be directly measured, one always explore properties of nuclear matter and the dynamical description of heavy-ion collisions through the analysis of the final-state products. As well known, the two-particle momentum correlation function, or called Hanbury-Brown Twiss (HBT) technique in the final-state has been used mostly as a probe of the space-time properties and characteristics of the emission source [26–28]. The two-proton momentum correlation function has been explored systematically by a lot of experiments and different models, several reviews can be found in Refs. [29–32]. In various HBT studies, effects of the impact parameter, the total momentum of nucleon pairs, the isospin of the emission source, the nuclear symmetry energy, the nuclear equation of state (EOS) as well as the in-medium nucleon-nucleon cross section has been discussed in the literature [33–39]. Even more, nuclear structure effects were also carefully investigated, such as the effects from binding energy and separation energy of the nucleus [40], density distribution of valence neutrons in neutron-rich nuclei [41], as well as high momentum tail of the nucleon-momentum distribution [42] etc. Two-proton momentum correlation function was also constructed in few-body reactions as well as α-clustered nucleus induced collisions [43–47]. In addition, two light charged particles momentum correlation function also offers a unique tool to investigate dynamical expansion of the reaction zone [39].

Here we extend the HBT method of final-state interaction to study the time-spatial information of the finite-temperature nuclear system. The purpose of the present paper is to systematically investigate the relationship between two-particle momentum correlation functions and system parameters, such as the source-temperature, density as well as system-size in a framework of the thermal isospin-dependent quantum molec-

*Corresponding author: mayugang@fudan.ac.cn

ular dynamics ($ThIQMD$) model [6, 15, 18]. In addition, Gaussian source radii are quantitatively extracted by assumption of Gaussian source fits to the HBT distributions. In this article, the evolution process of the excited nuclear source at an initial temperature varying from 1 MeV to 20 MeV are studied. The present work selects six different systems with similar ratio of neutron to proton numbers, *i.e.*, $N/Z \sim 1.3$, which include $(A, Z) = (36, 15)$, $(52, 24)$, $(80, 33)$, $(100, 45)$, $(112, 50)$, and $(129, 54)$. Then, Lednický-Lyuboshitz theoretical approach [48] is applied for calculating two-particle momentum correlation functions constructed based on phase-space information from the evolution process of the single excited nuclear source by the $ThIQMD$ model.

The rest of this article is organized as follows. In Section II, we firstly describe the thermal isospin-dependent quantum molecular dynamics model ($ThIQMD$) [15, 18], then briefly introduce the Hanbury-Brown and Twiss (HBT) technique using *Lednický* and *Lyuboshitz* analytical formalism. In Section III, we show the results of the $ThIQMD$ plus the LL method for the source-temperature dependence of two-particle momentum correlation function. The two-particle momentum correlation function and the influences of different temperature and system-size are systematically discussed. The detailed analysis of the extracted Gauss source radii are presented under different source-temperature and density. Furthermore, the momentum correlation function of two-neutron is also analyzed. Finally, Section IV gives a summary of the paper.

II. MODELS AND FORMALISM

A. THE ThIQMD MODEL

Since the two-particle momentum correlation functions are calculated in a specific application of the Lednický and Lyuboshitz theoretical simulation, the true single-particle phase-space distribution at the freeze-out stage is required. In this paper, the thermal isospin-dependent Quantum Molecular Dynamics transport model is used as the event generator, which has been applied successfully to study the $LGPT$ [6, 25]. In the following discussion, we introduce the modified model briefly. As well known, isospin-dependent Quantum Molecular Dynamics ($IQMD$) model was used to describe the collision process between two nuclei. The Quantum Molecular Dynamics transport model is a n-body transport theory, which describes heavy-ion reaction dynamics from intermediate to relativistic energies [49–53]. In the present work, we use a single excited source in the $ThIQMD$ which is different from the traditional $IQMD$. Usually, the ground state of the initial nucleus is considered to be $T = 0$ MeV in the traditional $IQMD$ model. However, the $ThIQMD$ model described by Fang, Ma, Zhou and Liu in Ref. [6, 15, 18], is used to simulate the single nuclear source at different temperature $T > 0$ MeV.

The main parts of QMD transport model include the following issues: the initialization of the projectile and the target, nucleon propagation under the effective potential, the collisions between the nucleons in the nuclear medium and the Pauli blocking effect. In the $ThIQMD$, instead of using the Fermi-Dirac distribution for $T = 0$ MeV, $P_F^i(\vec{r}) = \hbar \left[3\pi^2 \rho_i(\vec{r})\right]^{1/3}$, the initial momentum of the nucleons is sampled by the Fermi-Dirac distribution at finite temperature:

$$n\left(e_k\right) = \frac{g\left(e_k\right)}{e^{\frac{e_k-\mu}{T}}+1}, \tag{1}$$

where the kinetic energy $e_k = \frac{p^2}{2m}$, p and m is the momentum and mass of the nucleon, respectively. $g\left(e_k\right) = \frac{V}{2\pi^2}\left(\frac{2m}{\hbar^2}\right)^{\frac{3}{2}}\sqrt{e_k}$ represents the state density with the volume of the source $V = \frac{4}{3}\pi r^3 \left(r = r_0 A^{\frac{1}{3}}\right)$.

In addition, the chemical potential μ is determined by the following equation:

$$\frac{1}{2\pi^2}\left(\frac{2m}{\hbar^2}\right)^{\frac{3}{2}}\int_0^\infty \frac{1}{e^{\frac{e_k-\mu}{T}}+1} de_k = \rho_i. \tag{2}$$

In the $ThIQMD$ model, the interaction potential is also represented by the form as follows:

$$U = U_{Sky} + U_{Coul} + U_{Yuk} + U_{Sym} + U_{MDI}, \tag{3}$$

where U_{Sky}, U_{Coul}, U_{Yuk}, U_{Sym}, and U_{MDI} are the density-dependent Skyrme potential, the Coulomb potential, the surface Yukawa potential, the isospin asymmetry potential, and the momentum-dependent interaction, respectively. Among these potential, the Skyrme potential, the Coulomb potential and the momentum-dependent interaction can be written as follows:

$$U_{Sky} = \alpha(\frac{\rho}{\rho_0}) + \beta(\frac{\rho}{\rho_0})^\gamma, \tag{4}$$

where ρ and ρ_0 are total nucleon density and its normal value at the ground state, *i.e.*, 0.16 fm^{-3}, respectively. The above parameters α, β, and γ with an incompressibility parameter K are related to the nuclear equation of state [54–60].

$$U_{Sym} = C_{sym}\frac{(\rho_n - \rho_p)}{\rho_0}\tau_z, \tag{5}$$

$$U_{Coul} = \frac{1}{2}\left(1 - \tau_z\right)V_c, \tag{6}$$

where ρ_n and ρ_p are neutron and proton densities, respectively, τ_z is the z th component of the isospin degree of freedom for the nucleon, which equals 1 or -1 for a neutron or proton, respectively. And C_{sym} is the symmetry energy coefficient. U_{Coul} is the Coulomb potential where V_c is the Coulomb potential for protons.

$$U_{MDI} = \delta \cdot \ln^2\left(\epsilon \cdot (\Delta p)^2 + 1\right) \cdot \frac{\rho}{\rho_0}, \tag{7}$$

where Δp is the relative momentum, δ and ϵ can be found in Refs. [49, 50]. Their value of the above potential parameters are all listed in Table I:

TABLE I: The value of the interaction potential parameters.

α	β	γ	K	δ	ϵ
(MeV)	(MeV)		(MeV)	(MeV)	$((GeV/c)^{-2})$
-390.1	320.3	1.14	200	1.57	500

B. LEDNICKÝ AND LYUBOSHITZ ANALYTICAL FORMALISM

Next, we briefly review the method for the two-particle momentum correlation function proposed by Lednický and Lyuboshitz [48, 61, 62]. The main framework of the HBT technique is based on the principle as follows: when they are emitted at small relative momenta, the two-particle momentum correlation is determined by the space-time characteristics of the production processes owing to the effects of quantum statistics (QS) and final-state interactions (FSI) [63]. Therefore, the two-particle momentum correlation function can be expressed through a square of the symmetrizied Bethe-Salpeter amplitude averaging over the four coordinates of the emission particles and the total spin of the two-particle system, which represents the continuous spectrum of the two-particle state.

In this theoretical approach, the final-state interactions of the particle pairs is assumed independent in the production process. According to the conditions in Ref. [64], the correlation function of two particles can be written as the expression:

$$\mathbf{C}\left(\mathbf{k}^{*}\right)=\frac{\int \mathbf{S}\left(\mathbf{r}^{*},\mathbf{k}^{*}\right)\left|\Psi_{\mathbf{k}^{*}}\left(\mathbf{r}^{*}\right)\right|^{2}d^{4}\mathbf{r}^{*}}{\int \mathbf{S}\left(\mathbf{r}^{*},\mathbf{k}^{*}\right)d^{4}\mathbf{r}^{*}}, \tag{8}$$

where $\mathbf{r}^{*}=\mathbf{x}_{1}-\mathbf{x}_{2}$ is the relative distance of the two particles at their kinetic freeze-out, $\mathbf{k}^{*}$ is half of the relative momentum between two particles, $\mathbf{S}\left(\mathbf{r}^{*},\mathbf{k}^{*}\right)$ is the probability to emit a particle pair with given $\mathbf{r}^{*}$ and $\mathbf{k}^{*}$, *i.e.*, the source emission function, and $\Psi_{\mathbf{k}^{*}}\left(\mathbf{r}^{*}\right)$ is Bethe-Salpeter amplitude which can be approximated by the outer solution of the scattering problem [65]. In the above limit, the asymptotic solution of the wave function of the two charged particles approximately takes the expression:

$$\Psi_{\mathbf{k}^{*}}\left(\mathbf{r}^{*}\right)=e^{i\delta_{c}}\sqrt{A_{c}\left(\lambda\right)}\times \left[e^{-i\mathbf{k}^{*}\mathbf{r}^{*}}F\left(-i\lambda,1,i\xi\right)+f_{c}\left(k^{*}\right)\frac{\tilde{G}\left(\rho,\lambda\right)}{r^{*}}\right]. \tag{9}$$

In the above equation, $\delta_{c}=arg\,\Gamma\left(1+i\lambda\right)$ is the Coulomb s-wave phase shift with $\lambda=\left(k^{*}a_{c}\right)^{-1}$ where a_{c} is the two-particle Bohr radius, $A_{c}\left(\lambda\right)=2\pi\lambda\left[\exp\left(2\pi\lambda\right)-1\right]^{-1}$ is the Coulomb penetration factor, and its positive (negative) value corresponds to the repulsion (attraction). $\tilde{G}\left(\rho,\lambda\right)=\sqrt{A_{c}\left(\lambda\right)}\left[G_{0}\left(\rho,\lambda\right)+iF_{0}\left(\rho,\lambda\right)\right]$ is a combination of regular (F_{0}) and singular (G_{0}) s-wave Coulomb functions [61, 62]. $F\left(-i\lambda,1,i\xi\right)=1+\left(-i\lambda\right)\left(i\xi\right)/1!^{2}+\left(-i\lambda\right)\left(-i\lambda+1\right)\left(i\xi\right)^{2}/2!^{2}+\cdots$ is the confluent hypergeometric function with $\xi=\mathbf{k}^{*}\mathbf{r}^{*}+\rho$, $\rho=k^{*}r^{*}$.

$$f_{c}\left(k^{*}\right)=\left[K_{c}\left(k^{*}\right)-\frac{2}{a_{c}}h\left(\lambda\right)-ik^{*}A_{c}\left(\lambda\right)\right]^{-1} \tag{10}$$

is the s-wave scattering amplitude renormalizied by the long-range Coulomb interaction, with $h\left(\lambda\right)=\lambda^{2}\sum_{n=1}^{\infty}\left[n\left(n^{2}+\lambda^{2}\right)\right]^{-1}-C-\ln\left[\lambda\right]$ where $C=0.5772$ is the Euler constant. $K_{c}\left(k^{*}\right)=\frac{1}{f_{0}}+\frac{1}{2}d_{0}k^{*^{2}}+Pk^{*^{4}}+\cdots$ is the effective range function, where d_{0} is the effective radius of the strong interaction, f_{0} is the scattering length and P is the shape parameter. The parameters of the effective range function are important parameters characterizing the essential properties of the FSI, and can be extracted from the correlation function measured experimentally [39, 65–67].

For $n-n$ correlation functions which include uncharged particle, only the short-range particle interaction works. For $p-p$ correlation functions, both the Coulomb interaction and the short-range particle interaction dominated by the s-wave interaction are considered.

III. ANALYSIS AND DISCUSSION

Within the framework of the thermal isospin-dependent quantum molecular dynamics model [6, 15, 18], the two-particle momentum correlation functions are calculated by using the phase-space information from the freeze-out stage of the excited nuclear source at an initial temperature varying from 1 MeV to 20 MeV and/or density varying from $\rho=0.2\rho_{0}$ to $1.2\rho_{0}$. This work performs calculations for thermal source systems with different mass including $(A,Z)=(36,15),(52,24),(80,33),(100,45),(112,50)$, and $(129,54)$.

We firstly calculated the proton-proton momentum correlation function $C_{pp}(q)$ for a finite-size systems at temperatures ranging from 1 to 20 MeV. In Fig. 1, the results of $C_{pp}(q)$ for temperature of 2, 4, 6, 8, 10 and 12 MeV at different values of density ($0.2\rho_{0}$ - $1.2\rho_{0}$) are presented. The proton-proton momentum correlation function exhibits a peak at relative momentum $q=20$ MeV/c, which is due to the strong final-state s-wave attraction together with the suppression at lower relative momentum as a result of Coulomb repulsion and the anti-symmetrization wave function between two protons. The shape of the two-proton momentum correlation functions is consistent with previous experimental data in heavy-ion collisions [68]. For protons which are emitted from the lower temperature ($T<8$ MeV) source in Fig. 1 (a)-(c), the general trend is very similar. The figure shows that $C_{pp}(q)$ increases as ρ increases for fixed T ($T<8$ MeV). The increase of the density indicates that the geometrical size becomes smaller for a source with fixed neutrons and protons, which makes the strength of the

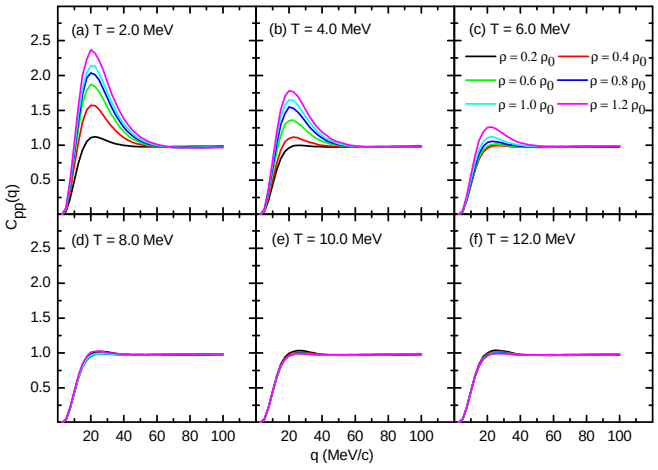

FIG. 1: The proton-proton momentum correlation functions ($C_{pp}(q)$) at different densities (*i.e.*, $0.2\rho_0$, $0.4\rho_0$, $0.6\rho_0$, $0.8\rho_0$, $1.0\rho_0$, and $1.2\rho_0$) for the smaller nucleus (A=36, Z=15) with fixed source-temperatures T = 2 MeV (a), 4 MeV (b), 6 MeV (c), 8 MeV (d), 10 MeV (e) and 12 MeV (f), respectively. The freeze-out time is taken to be 200 fm/c.

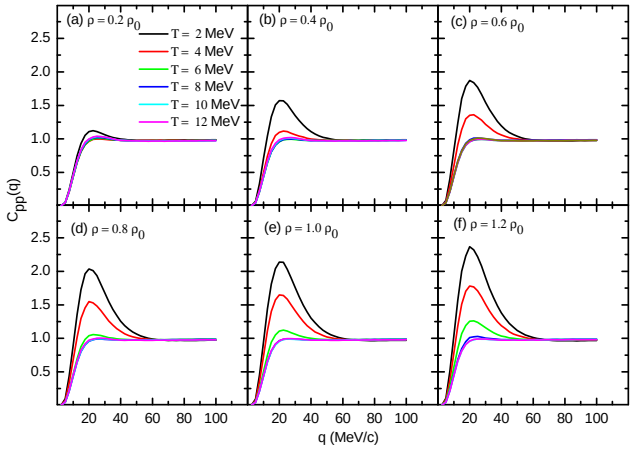

FIG. 2: Similar to Fig. 1, but at different source-temperatures (T = 2, 4, 6, 8, 10 and 12 MeV) with different fixed densities, namely $\rho = 0.2\rho_0$ (a), 0.4 ρ_0 (b), 0.6 ρ_0 (c), 0.8 ρ_0 (d), 1.0 ρ_0 (e), and $1.2\rho_0$ (f).

momentum correlation function larger. Finally, the p-p momentum correlation function become almost one at $q > 60$ MeV/c. For larger T ($T > 8$ MeV) in Fig. 1 (d)-(f), the difference of $C_{pp}(q)$ between different densities becomes smaller. From Fig. 1, it is found that the $C_{pp}(q)$ is almost the same after $T = 8$ MeV for different densities and the $p-p$ momentum correlation function becomes almost one above approximately $q = 30$ MeV/c. It indicates that the emitted proton is not affected by the change of density when the source temperature beyond certain value ($T \approx 8$ MeV in present work). In order to understand which one of the two factors (*i.e.*, temperature and density) has larger influence, the two-particle

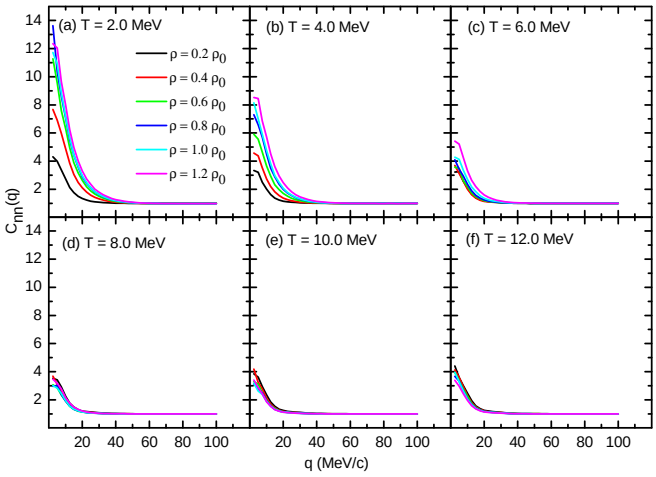

FIG. 3: The neutron-neutron (n-n) momentum correlation function ($C_{nn}(q)$) in the same conditions as Fig. 1.

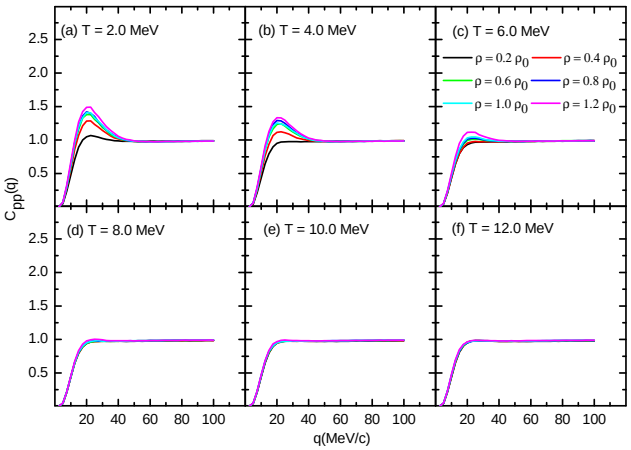

FIG. 4: Same to Fig. 1, but for a larger system (A=129,Z=54).

momentum correlation in fig. 2 is plotted by exchanging of the two input parameters. From fig. 2, we can intuitively observe dependence of the two-particle momentum correlation on the source temperature. The dependence of $C_{pp}(q)$ on the source temperature is stronger than on density. In other words, the $C_{pp}(q)$ is more sensitive to T than to density ρ. In addition, for larger ρ from fig. 2 (a) to (f), the difference of $C_{pp}(q)$ between different densities becomes bigger. Next, we explore whether the phenomenon exists in momentum correlation of the uncharged-particle pairs. Fig. 3 presents the neutron-neutron momentum correlation functions ($C_{nn}(q)$) for temperature of 2, 4, 6, 8, 10 and 12 MeV at different values of density, respectively. For neutron-neutron momentum correlation function, it peaks at $q \approx 0$ MeV/c caused by the s-wave attraction. Although the $C_{nn}(q)$ has different shape compared with the $p-p$ momentum correlation, it has the similar dependence on the source

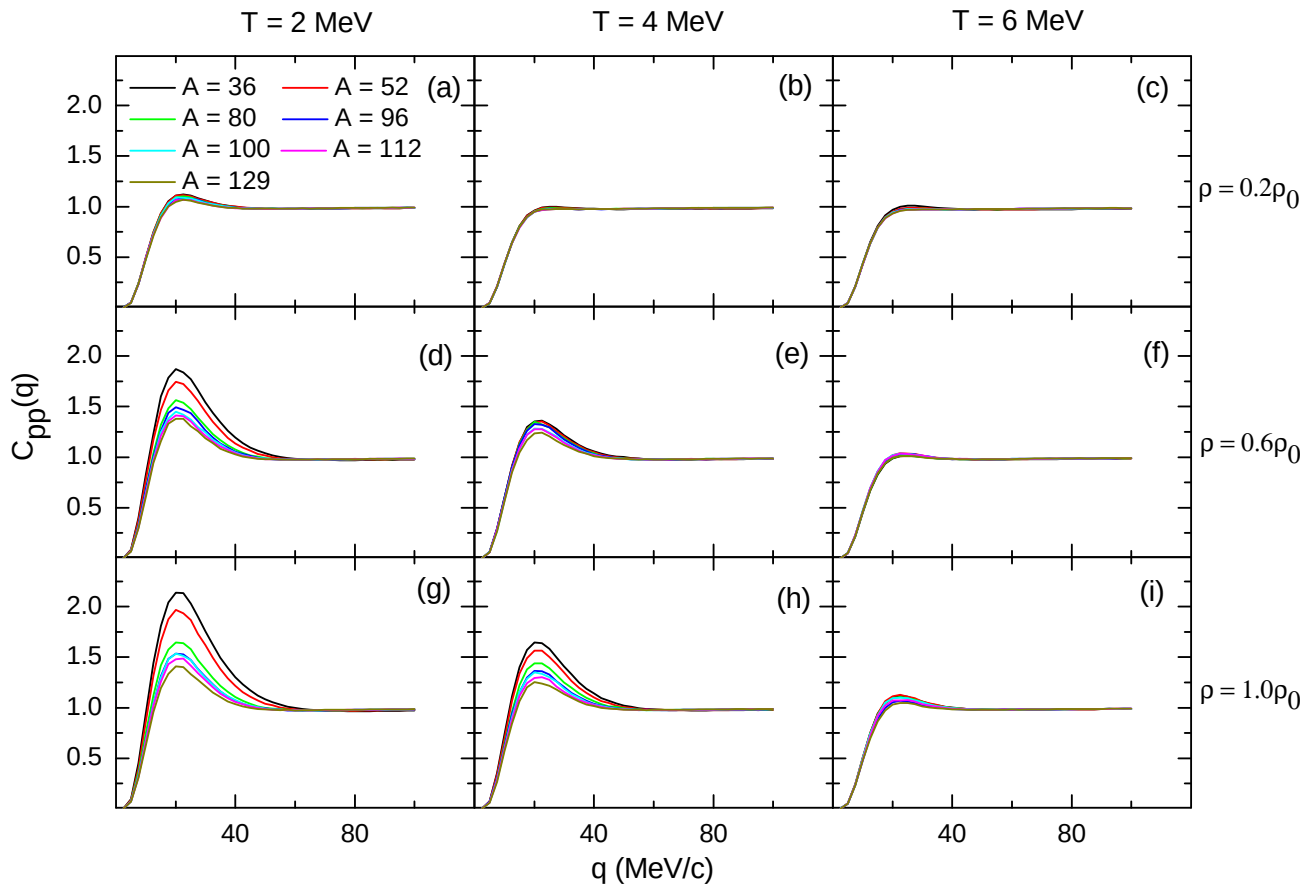

FIG. 5: $C_{pp}(q)$ of different source size system at fixed temperatures (i.e., from left column to right column, they correspond to $T = 2$, 4 and 6 MeV, respectively) or fixed densities (i.e., from top row to bottom row, they correspond to $\rho = 0.2\rho_0$, $0.4\rho_0$, $0.6\rho_0$, respectively).

temperature and density. The similar trend in $C_{pp}(q)$ and $C_{nn}(q)$ shows the close emission mechanism in the evolution process.

Fig. 4 shows the results of a larger system at different source-temperature and density and a similar behavior of $C_{pp}(q)$ is demonstrated. We also observe that the proton-proton momentum correlation in larger-size system ($(A, Z) = (129, 54)$) in Fig. 4 becomes weaker compared to the smaller-size source ($(A, Z) = (36, 15)$) in Fig. 1. In view of the above phenomenon, Fig. 5 describes the relationship between system-size and momentum correlation function in more details. The decreasing of $C_{pp}(q)$ as the system-size increasing for a fixed value of T or ρ can be clearly seen in Fig. 5 (g), which is consistent with the previous results of Gaussian source [38, 39, 69]. In Fig. 5 (a)-(i), with larger temperature or lower density, the difference of $C_{pp}(q)$ between different T or ρ becomes smaller, respectively. The Gaussian source radii are extracted for further discussion later in this article.

From the above plots, we can extract $C_{max}(q)$, *i.e.*, the maximum value of $C_{pp}(q)$ as well as the full width at half maximum ($FWHM$) of $C_{pp}(q)$ distribution, *i.e.* at $C_{pp}(q) = [C_{max}(q) - 1]/2$. The source-temperature T dependence of $C_{max}(q)$ and $FWHM$ for the proton-proton momentum correlation function with different density are given in Fig. 6. As shown in Fig. 6 (a) and (b), both $C_{max}(q)$ and $FWHM$ decrease gradually with increasing T. In addition, both of them increase gradually with increasing density. At high temperature, the change of $C_{max}(q)$ and $FWHM$ is very small and not plotted in the figure. Of course, the behavior of the $C_{max}(q)$ and $FWHM$ with T and ρ can also be cleanly seen in Fig. 2, and the increasing of $C_{max}(q)$ and $FWHM$ are generally inversely proportional to Gaussian radius r_0 as shown later. Similarly, the system-size A dependence of $C_{max}(q)$ and $FWHM$ for the proton-proton momentum correlation function at $T = 2MeV$ and $\rho = 0.6\rho_0$ is shown in Fig. 7. The dependence of $C_{max}(q)$ and $FWHM$ on system-size A is quite similar to the temperature dependence in Fig. 6. The $C_{max}(q)$ and $FWHM$ values become smaller for systems with larger size.

Fig. 8 shows the source-temperature, density, and

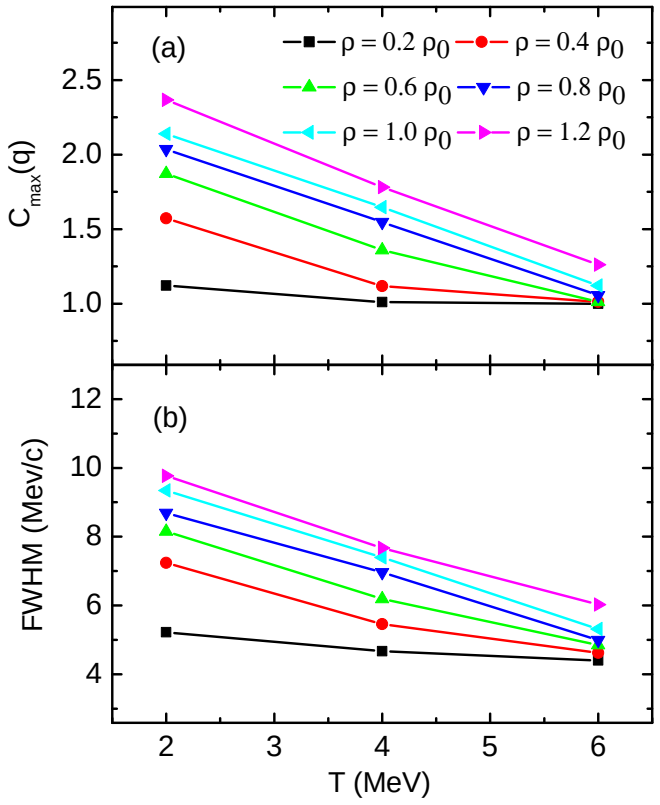

FIG. 6: Source-temperature T dependence of $C_{max}(q)$ (a) and of $FWHM$ (b) of $C_{pp}(q)$ distributions at different densities ($0.2\rho_0$ - $1.2\rho_0$) for the ($A = 35$, $Z = 16$) system.

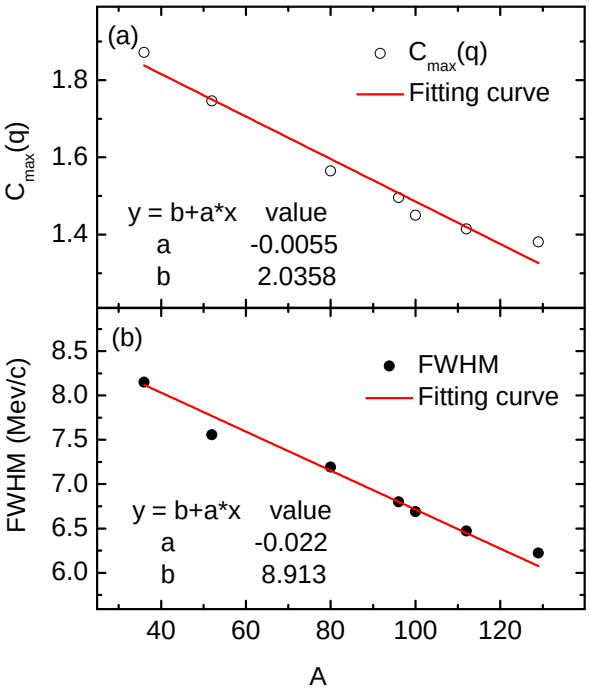

FIG. 7: $C_{max}(q)$ (a) and $FWHM$ (b) for different source-size systems at given $T = 2\ MeV$ and $\rho = 0.6\rho_0$.

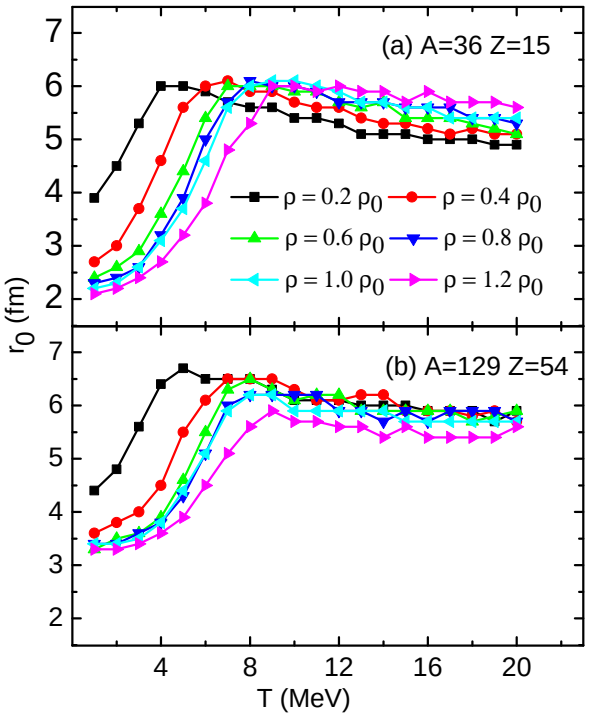

FIG. 8: Gaussian source radius as a function of temperature at different density ($\rho = 0.2\rho_0$, $0.4\rho_0$, $0.6\rho_0$, $0.8\rho_0$, $1.0\rho_0$, $1.2\rho_0$) for a fixed source size. Panels (a) and (b) correspond to the smaller source size with ($A = 36$, $Z = 15$) and the larger source size with ($A = 129$, $Z = 54$), respectively.

system-size dependence of Gaussian radii extracted from two-particle momentum correlation functions, where panels (a) and (b) are results with the smaller source size and the larger source size, respectively. The radii are extracted by a Gaussian source assumption, *i.e.*, $S(r) \approx \exp[-r^2/(4r_0^2)]$, where r_0 is the Gaussian source radius from the proton-proton momentum correlation functions. The theoretical calculations for $C_{pp}(q)$ was performed by using the *Lednický* and *Lyuboshitz* analytical method. The best fitting radius is judged by finding the minimum of the reduced chi-square between the $ThIQMD$ calculations and the Gaussian source assumption. It can be observed that the Gaussian radius increases initially and then decreases slightly after taking a maximum value at a certain temperature in Fig. 8. As the density decreases, the decreasing speed of the Gaussian radius of the small system is larger than that of the larger system. Fig. 9 shows the Gaussian radius of the different system-size varies with the temperature in panels (a)-(c) or density in panels (d)-(f). The Gaussian source radius is consistent with the system-size, *i.e.*, at higher temperature or larger density, the differences of Gaussian source between different system sizes are bigger in the low density and low temperature region, but the difference in opposite conditions almost disappear.

From the above discussion, it is demonstrated that the strength of the two-particle momentum correlation

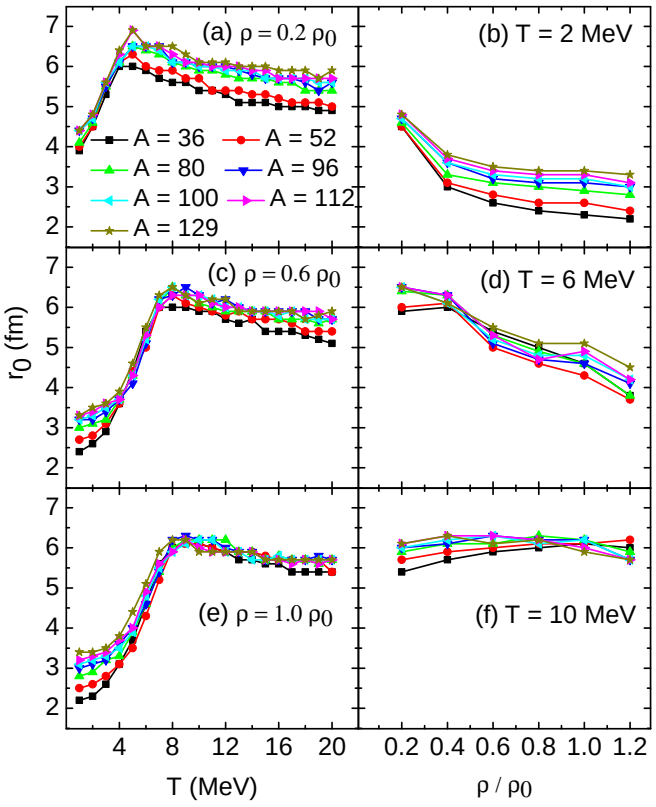

FIG. 9: Gaussian source radius as a function of temperature or density at different source-size systems. Left and right column correspond to the density ($\rho = 0.2\rho_0$, $0.6\rho_0$, $1.0\rho_0$) and the temperature ($T = 2$, 6, 10 MeV), respectively.

function is affected by the source temperature, density and system size. The two-particle momentum correlation function strength is larger for a single source with lower temperature, higher density or smaller mass number as shown in Fig. 1-5. Otherwise, the strength becomes smaller. To some extents, the strong correlation between two particles is mainly caused by the closing position of each other in phase space in both coordinate and momentum. Varying only one in the three condition parameters (temperature, density and system size), lower temperature means smaller momentum space, higher density means smaller coordinate space and small system size also mean smaller coordinate space to keep fixed density compared with large system size. The dependencies of the two-particle momentum correlation function strength on the source temperature, density and system size could be explained by the change of the phase space sizes. Two particles emitted from small phase space will have strong correlation and those from large phase space will have weak correlation. For example, the increase of the $C_{pp}(q)$ strength with the increase of the density for a fixed system size could be explained by the decreasing of the coordinate space as shown in Fig. 1 (a). And the small $C_{pp}(q)$ strength at temperature higher than 8 MeV could be caused by the large momentum space compared with lower temperatures as shown in Fig. 1 (d-f). The decrease of the $C_{pp}(q)$ strength with the increase of the system size for a fixed density could also be explained by the increasing of the coordinate space as shown in Fig. 5 (g). Thus it could be concluded that the phase space size for the emitted nucleons have strong effect on strength of the two-particle momentum correlation function, which can also be seen in the extracted Gaussian radii as shown in Fig. 8. However, the sensitivities to the source radii seem to be different in the different regions of temperatures and densities. For example, the temperature sensitivity are better in the lower region at fixed density, and so does for density sensitivity at lower temperatures.

IV. SUMMARY

In summary, the two-particle momentum correlation functions for a single excited source are investigated using the Lednický and Lyuboshitz analytical formalism with the phase-space points at the freeze-out stage for different initial temperature and density in a framework of the $ThIQMD$ transport approach. We mainly performed a series of studies focused on the varied effects of source temperature, density and system-size on the two-particle momentum correlation functions. The results reflect that the shape of the two-proton momentum correlation function is in accordance with the previous experimental data in heavy-ion collisions [68]. At the same time, the trend of the relationship between the two-proton momentum correlation and system-size is consistent with previous simulation [38, 39, 69]. At low source-temperature, the larger density makes the two-particle momentum correlation stronger. However, at higher source temperature, the effect becomes almost disappear. Both protons and neutrons have the similar behavior. This work also shows that the emitted particles are not influenced by density above a given temperature in a single excited source. In the same way, the emitted particles are softly influenced by temperature below a given density in single excited source. In one word, the dependence of the two-particle momentum correlation function on the source temperature, density and system size could be explained by the change of the coordinate and/or momentum phase space sizes. In the end, the Gaussian radius is extracted to explore the emission source size in single excited system. Gaussian radius becomes larger in the larger system. The dependence of the extracted Gaussian radius on source-temperature and density is consistent with behavior of the two-proton momentum correlation function as discussed in the texts.

Acknowledgments

This work was supported in part by the National Natural Science Foundation of China under contract Nos.

11890710, 11890714, 11875066, 11925502, 11961141003, 11935001, 12147101 and 12047514, the Strategic Priority Research Program of CAS under Grant No. XDB34000000, National Key R&D Program of China under Grant No. 2016YFE0100900 and 2018YFE0104600, Guangdong Major Project of Basic and Applied Basic Research No. 2020B0301030008, and the China PostDoctoral Science Foundation under Grant No. 2020M681140.

[1] G. Giuliani, H. Zheng, and A. Bonasera, Prog. Part. Nucl. Phys. **76**, 116 (2014).
[2] B. A. Li, L. W. Chen, and C. M. Ko, Phys. Rep. **464**, 113 (2008).
[3] B. Borderie and M. F. Rivet, Prog. Part. Nucl. Phys. **61**, 551 (2008).
[4] C. W. Ma and Y.-G. Ma, Prog. Part. Nucl. Phys. **99**, 120(2018).
[5] Y. G. Ma and W. Q. Shen, Nucl. Sci. Tech. **15**, 4 (2004).
[6] H. L. Liu, Y. G. Ma, and D. Q. Fang, Phys. Rev. C **99**, 054614 (2019).
[7] J. E. Finn, S. Agarwal, A. Bujak *et al.*, Phys. Rev. Lett. **49**, 1321 (1982).
[8] P. J . Siemens, Nature **305**, 410 (1983).
[9] Y. G. Ma, A. Siwek, J. Péter *et al.*, Phys. Lett. B **390**, 41 (1997).
[10] Y. G. Ma, Phys. Rev. Lett. **83**, 3617 (1999).
[11] P. Chomaz, V. Duflot, F. Gulminelli, Phys. Rev. Lett. **85**, 3587 (2000).
[12] J. B. Natowitz, K. Hagel, Y. G. Ma, M. Murray, L. Qin, R. Wada, J. Wang, Phys. Rev. Lett. **89**, 212701 (2002).
[13] Y. G. Ma, J.B. Natowitz, R. Wada *et al.*, Phys. Rev. C **71**, 054606 (2005).
[14] B. Borderie, J. Frankland, Prog. Part. Nucl. Phys. **105**, 82 (2019).
[15] Zhen-Fang Zhang, De-Qing Fang,and Yu-Gang Ma, Nucl. Sci. Tech. **29**, 78 (2018).
[16] N. Auerbach, S. Shlomo, Phys. Rev. Lett. **103**, 172501 (2009).
[17] N. D. Dang, Phys. Rev. C **84**, 034309 (2011).
[18] D. Q. Fang, Y. G. Ma, C. L. Zhou, Phys. Rev. C **89**, 047601 (2014).
[19] X. G. Deng, Y. G. Ma, M. Veselský, Phys. Rev. C **94**, 044622 (2016).
[20] D. Mondal, D. Pandit, S. Mukhopadhyay *et al.*, Phys. Rev. Lett. **118**, 192501 (2017).
[21] A. Bracco, J.J. Gaardhje, A.M. Bruce *et al.*, Phys. Rev. Lett. **62**, 2080 (1989).
[22] P.F. Bortignon, A. Bracco, D. Brink, R.A. Broglia, Phys. Rev. Lett. **67**, 3360 (1991).
[23] O. Wieland, A. Bracco, F. Camera *et al.*, Phys. Rev. Lett. **97**, 012501 (2006).
[24] Rui Wang, Yu-Gang Ma, R. Wada *et al.*, Phys. Rev. Res. **2**, 043202 (2020).
[25] Y. D. Song, R. Wang, Y. G. Ma, X. G. Deng, H. L. Liu, Physics Letters B **814**, 136084 (2021).
[26] R. Kotte *et al.*, Eur. Phys. J. A **23**, 271 (2005).
[27] R. Ghetti *et al.*, Phys. Rev. Lett. **91**, 092701 (2003).
[28] D. Gourio *et al.*, Eur. Phys. J. A **7**, 245 (2000).
[29] D. H. Boal, C. K. Gelbke, B. K. Jennings, Rev. Mod. Phys. **62**, 553 (1990).
[30] U. A. Wiedemann, U. Heinz, Phys. Rep. **319**, 145 (1999).
[31] M. A. Lisa, S. Pratt, R. Soltz, U. Wiedemann, Ann. Rev. Nucl. Part. Sci. **55**, 357 (2005).
[32] G. Verde, A. Chbihi, R. Ghetti, J. Helgesson, Eur. Phys. J. A **30**, 81 (2006).
[33] W. G. Gong, W. Bauer, C. K. Gelbke, and S. Pratt, Phys. Rev. C **43**, 781 (1991).
[34] G. Verde, D. A. Brown, P. Danielewicz, C. K. Gelbke, W. G. Lynch, and M. B. Tsang, Phys. Rev. C **65**, 054609 (2002).
[35] Y. G. Ma *et al.*, Phys. Rev. C **73**, 014604 (2006).
[36] R. Ghetti *et al.*, Phys. Rev. C. **69**, 031605(R) (2004).
[37] L. W. Chen, V. Greco, C. M. Ko, and B. A. Li, Phys. Rev. Lett. **90**, 162701 (2003).
[38] Ting-Ting Wang, Yu-Gang Ma, Chun-Jian Zhang and Zheng-Qiao Zhang, Phys. Rev. C **97**, 034617 (2018).
[39] Ting-Ting Wang, Yu-Gang Ma, and Zheng-Qiao Zhang, Phys. Rev. C **99**, 054626 (2019).
[40] Y. B. Wei, Y. G. Ma, W. Q. Shen *et al.*, Phys. Lett. B **586**, 225 (2004).
[41] X. G. Cao, X. Z. Cai, Y. G. Ma, D. Q. Fang, G. Q. Zhang, W. Guo, J. G. Chen, and J. S. Wang, Phys. Rev. C **86**, 044620 (2012).
[42] Gao-Feng Wei, Xi-Guang Cao, Qi-Jun Zhi, Xin-Wei Cao, and Zheng-Wen Long, Phys. Rev. C **101**, 014613 (2020).
[43] B. S. Huang, Y. G. Ma, Phys. Rev. C **101**, 034615 (2020).
[44] D. Q. Fang, Y. G. Ma, X. Y. Sun *et al.*, Phys. Rev. C **94**, 044621 (2016).
[45] Bo-Song Huang, Yu-Gang Ma, Chin. Phys. C **44**, 094105 (2020).
[46] L. Shen, B. S. Huang, Y. G. Ma, Phys. Rev. C accepted, (2021).
[47] J. J. He, S. Zhang, Y. G. Ma, J. H. Chen, C. Zhong, Eur. Phys. J. A **56**, 52 (2020).
[48] R. Lednický, Nucl. Phys. A **774**, 189 (2006).
[49] J. Aichelin, A. Rosenhauer, G. Peilert, H. Stoecker, and W. Greiner, Phys. Rev. Lett. **58**, 1926 (1987).
[50] J. Aichelin, Phys. Rep. **202**, 233 (1991).
[51] G. Peilert, H. *Stöcker*, W. Greiner, A. Rosenhauer, A. Bohnet, and J. Aichelin, Phys. Rev. C **39**, 1402 (1989).
[52] Peng-Cheng Li, Yong-Jia Wang, Qing-Feng Li, Hong-Fei Zhang, Nucl. Sci. Tech. **29**, 177 (2018).
[53] Zhao-Qing Feng, Nucl. Sci. Tech. **29**, 40 (2018).
[54] Bao-An Li, Lie-Wen Chen, Che Ming Ko, Phys. Rep. **464**, 113 (2008).
[55] J. Liu *et al.*, Nucl. Sci. Tech. **32**, 117 (2021).
[56] Fan Zhang, Jun Su, Nucl. Sci. Tech. **31**, 77 (2020) .
[57] Hao Yu, De-Qing Fang, Yu-Gang Ma, Nucl. Sci. Tech. **31**, 61 (2020).
[58] Gao-Feng Wei, Qi-Jun Zhi , Xin-Wei Cao, Zheng-Wen Long, Nucl. Sci. Tech. **31**, 71 (2020) .
[59] Chong-Ji Jiang, Yu Qiang, Da-Wei Guan*et al.*, Chin. Phys. Lett. **38**, 052101 (2021) .
[60] Jun Xu, Chin. Phys. Lett. **38**, 042101 (2021) .
[61] R. Lednický, Phys. Part. Nucl. **40**, 307 (2009).
[62] R. Lednický, Phys. Ato. Nucl. **71**, 1572 (2008).
[63] S. E. Koonin, Phys. Lett. B **70**, 43 (1977).
[64] R. Lednický, V.L. Lyuboshitz, B. Erazmus, and D. Nouais, Phys. Lett. B **373**, 30 (1996).

[65] L. Adamczyk *et al.* (STAR Collaboration), Nature **527**, 345 (2015).
[66] B. Erazmus, L. Martin, R. Lednicky, N. Carjan, Phys. Rev. C **49**, 349 (1994).
[67] J. Arvieux, Nucl. Phys. A **221**, 253 (1974).
[68] R. Ghetti *et al.*, Nucl. Phys. A **674**, 277 (2000).
[69] Long Zhou, De-Qing Fang, Nucl. Sci. Tech. **21**, 52 (2020).